Translational Oncology
www.transonc.com

Volume 10 Number 5 October 2017 pp. 831–838 831

Intravoxel Incoherent Motion Diffusion-weighted Imaging: Evaluation of the Differentiation of Solid Hepatic Lesions

Ma Luo[1], Ling Zhang[1], Xin-hua Jiang and Wei-dong Zhang

Department of Radiology, Sun Yat-sen University Cancer Center, State Key Laboratory of Oncology in South China, Collaborative Innovation Center for Cancer Medicine, Guangzhou, Guangdong 510060, PR China

Abstract

PURPOSE: To evaluate whether intravoxel incoherent motion (IVIM)–related parameters could be used to differentiate malignant from benign focal liver lesions (FLLs) and to improve diagnostic efficiency. *METHODS:* Seventy-four patients with 75 lesions, including 51 malignant FLLs and 24 benign FLLs, underwent liver 3.0-T magnetic resonance imaging for routine examination sequences. IVIM diffusion-weighted imaging (DWI) with 11 *b* values (0-800 s/mm^2) was also acquired concurrently. Apparent diffusion coefficient (ADC_{total}) and IVIM-derived parameters, such as the pure diffusion coefficient (*D*), the pseudodiffusion coefficient (*D*), and the perfusion fraction (*f*), were calculated and compared between the two groups. A receiver operating characteristic curve analysis was performed to assess their diagnostic value. *RESULTS:* ADC_{total}, *D*, and *f* were significantly lower in the malignant group than in the benign group, whereas *D* did not show a statistical difference. *D* had a larger area under the curve value (0.968) and higher sensitivity (92.30%) for differentiation. *CONCLUSION:* IVIM is a useful method to differentiate malignant and benign FLLs. The *D* value showed higher efficacy to detect hepatic solid lesions.

Translational Oncology (2017) 10, 831–838

Introduction

With advances in technology and the more widespread use of imaging, focal liver lesions (FLLs) are being encountered increasingly during routine clinical work. FLLs can be divided into malignant and benign as the two main entities. Benign lesions comprise hemangioma, focal nodular hyperplasia (FNH), cysts, adenomas, and angioleiomyolipoma (AML). The primary hepatic malignant tumors include hepatocellular carcinoma (HCC), cholangiocarcinoma, cystadenocarcinoma, and hepatoblastoma. Among them, HCC has the highest morbidity in the primary category in Asia, whereas metastasis, the most common liver tumor in secondary disease, outnumbers primary hepatic tumors, especially in the Western world. It is imperative for malignant lesions to be treated actively and emergently. Most benign lesions are asymptomatic and are not discovered until a routine health checkup or incidental imaging examination is performed. For benign lesions, the management ranges from surveillance to biopsy when necessary. However, malignant and benign liver lesions sometimes have indistinct characteristics that make an accurate diagnosis difficult, leading to misdiagnosis, conservative treatment, or even overintervention in the course of the disease. Therefore, an accurate diagnosis that differentiates benign from malignant lesions is of importance.

Magnetic resonance imaging (MRI) offers preferable advantages over computed tomography (CT), such as improved soft tissue contrast and lesion determination [1]. The characterization of most lesions is based upon contrast enhancement patterns. However, time consumption, cost, and anaphylactic reaction are major drawbacks of MRI, especially for liver-specific contrast agents. Diffusion-weighted imaging (DWI), as a noninvasive functional imaging technique, has played an important role in lesion detection because of its high sensitivity to water molecular mobility. Besides, because of its shorter

Address all correspondence to: Wei-dong Zhang, MD, 651 Dongfengdong Road, Guangzhou, Guangdong 510060, PR China.
E-mail: zhangwd@sysucc.org.cn
[1] Both authors contributed equally to this work.
Received 27 June 2017; Revised 10 August 2017; Accepted 10 August 2017

1936-5233/17
http://dx.doi.org/10.1016/j.tranon.2017.08.003

scanning time and lack of contrast medium, DWI has been widely applied in clinical practice [2,3]. The apparent diffusion coefficient (ADC) is a quantization parameter that is calculated by DWI according to two *b* values. In tissues with higher density of cellularity or tortuosity of the extracellular space, the diffusion of water protons is impeded. In such an environment, water movement is said to be "restricted," and the ADC is lowered. By contrast, in cystic or incompact tissues, the diffusion of water is free, and the ADC is higher. Thus, DWI is a unique tool that provides information on tissue cellularity, and the ADC represents the pathophysiological changes *in vivo* in a noninvasive way.

Nevertheless, after proving that a perfusion component existed inherently in DWI voxels that has a subtle influence on the ADC measurement, intravoxel incoherent motion (IVIM) was proposed initially by Le Bihan et al. [4]. This implied that the ADC was contaminated by the bloodstream instead of reflecting the pure diffusion in each voxel; thus, the ADC obtained from a traditional monoexponential process was larger than the true diffusion in voxels, indicating that the ADC might overlap between benign and malignant lesions, thereby eclipsing its efficacy. They demonstrated that both diffusion and perfusion could be assessed quantitatively and separately by multiple *b* values encompassing sufficient low and high values, according to a biexponential model.

IVIM incorporates the pure diffusion coefficient (D), the pseudodiffusion coefficient (D^*), and the perfusion fraction (f), respectively. IVIM has attracted much attention and has been applied for various medical purposes, such as therapeutic response evaluation [5], long-term outcome prediction [6], and chronic disease assessment [7], demonstrating great performance and excellent function. However, some studies showed that the performance of ADC is somewhat better than IVIM, being simpler and less prone to errors in the calculation process, resulting in higher efficacy in differentiation [8–10], as was shown by Zhu et al. that the differentiation performance, sensitivity, and specificity of ADC were 0.983, 96.97%, and 93.75% respectively, which were larger and higher than those for IVIM of 0.837, 87.88%, and 81.25%, respectively. Doblas et al. also supported these conclusions in a study that compared the two techniques among various liver diseases. Thus, ADC remains an important indicator in certain clinical work. The value of ADC and IVIM has not been determined because there is still no unanimous agreement on them, particularly to differentiate between benign and malignant liver lesions.

In this study, we used our data to determine the value of ADC and IVIM-related parameters to differentiate between benign and malignant solid hepatic tumors.

Materials and Methods

Study Selection

This study protocol was approved by the local ethics committee. Informed consent was acquired from all patients before the MRI examination. Between January 2016 and September 2016, clinically suspected FLLs were examined among 74 patients (62 men, 12 women) using CT or MRI. The exclusion criteria were as follows: 1) there was no liver nodule or tumor on CT or MRI; 2) the lesion diameter was less than 1 cm; 3) patients with FLLs treated by transarterial chemoembolization, radiofrequency ablation, or chemotherapy before the MRI examination; and 4) patients whose images were of unacceptable quality that interfered with the delineation of FLLs.

The final study population comprised 51 malignant FLLs and 24 benign FLLs. In the malignant group, there were 44 HCCs, 7 with metastasis. The benign group comprised 16, 6, and 2 hemangiomas, FNHs, and angioleiomyolipomas, respectively. The mean age of the malignant group was 52.31 ± 12.11 years (range: 23-79 years), whereas the mean age of the benign group was 47.50 ± 13.12 years (range: 27-84 years). Histopathological confirmation was available in 35 lesions, including 22 HCCs (13 patients after surgery and 9 patients by biopsy), 1 hemangioma, 2 angioleiomyolipomas, 7 metastases (all patients by biopsy), and 3 FNHs. In the remaining patients, the lesion was diagnosed by its typical imaging features according to the guidelines of the American Association for the Study of Liver Diseases, as well as by elevated alpha fetal protein in HCCs.

Data Acquisition

Regular MRI of the Liver. The patients were scanned prospectively by a 3.0-T MRI scanner (Discovery 750 W; GE Healthcare, Milwaukee, WI) with a 16-element body coil. The scanning comprised axial fat-suppressed respiratory-triggered (RT) propeller T2WI [repetition time (TR)/echo time (TE) 8000-10,000/96-100, slice/gap 5/1 mm, field of view (FOV) 40 cm], coronal RT T2WI (TR/TE 2000/70 for coronal, slice/gap 5/1 mm, FOV 36 cm), breath-hold axial in- and opposed-phase T1WI (TR/TE 4.0/2.2-1.1, slice/gap 1/1 mm), axial 3D GRE T1WI (LAVA, TR/TE 5.25/1.7, slice thickness 1/1 mm, FOV 38 cm), and contrast injection [0.01 mmol/kg of gadopentetate dimeglumine (n = 62; Magnevist, Bayer Shering Pharma, Berlin, Germany) and a 10-ml fixed dose of gadoxetic acid (n = 13; Primovist; Bayer Shering Pharma, Berlin, Germany)]. Postcontrast images were collected at the arterial phase (20 seconds), portal venous phase (60 seconds), and delayed phase (180 seconds). Hepatobiliary phase images were acquired at 20 minutes in patients injected with Primovist.

Parameters for DWI. RT DWI echo-planar imaging (EPI) with multiple *b* values was carried out. For patients administrated with Primovist, the DWI was performed before the hepatobiliary phase (about 20 minutes after the injection). For the remaining patients executing Magnevist administration, DWI was obtained precontrast. The image parameters were as follows: TR/TE 6000-10,000/61-64 milliseconds; FOV 40 × 40 cm; 15 slices, slice thickness/gap = 5/1 mm; spectral fat saturation; ASSET acceleration factor of two; *b* values = 0, 10, 20, 30, 50, 80, 100, 200, 400, 600, and 800 s/mm^2; and number of excitations = 3. There were three orthogonal gradient directions. The total average acquisition time of DWI was about 5 minutes.

Image Analysis

To obtain ADC_{total} and IVIM-related parameters, one or several regions of interest (ROIs) were placed by an abdominal radiologist on DWI at the b_0 image for each targeted lesion. If a lesion manifested homogeneity (Figure 1), a freehand ROI was drawn cautiously along the edge of the lesion to encompass as much of it as possible on the largest slice while avoiding surrounding vessels or bile ducts structures seen macrographically. If a lesion demonstrated a heterogeneous appearance (Figure 2), three identical circular ROIs were set on the largest slice to measure viable parts of tumor; care was taken to avoid necrosis or hemorrhagic areas and artifacts.

IVIM could be expressed by a mathematical formula according to the relationship between signal intensities and *b* values:

$$S_b/S_0 = (1-f)\ \exp.(-bD) + f\ \exp(-bD^*), \quad (1)$$

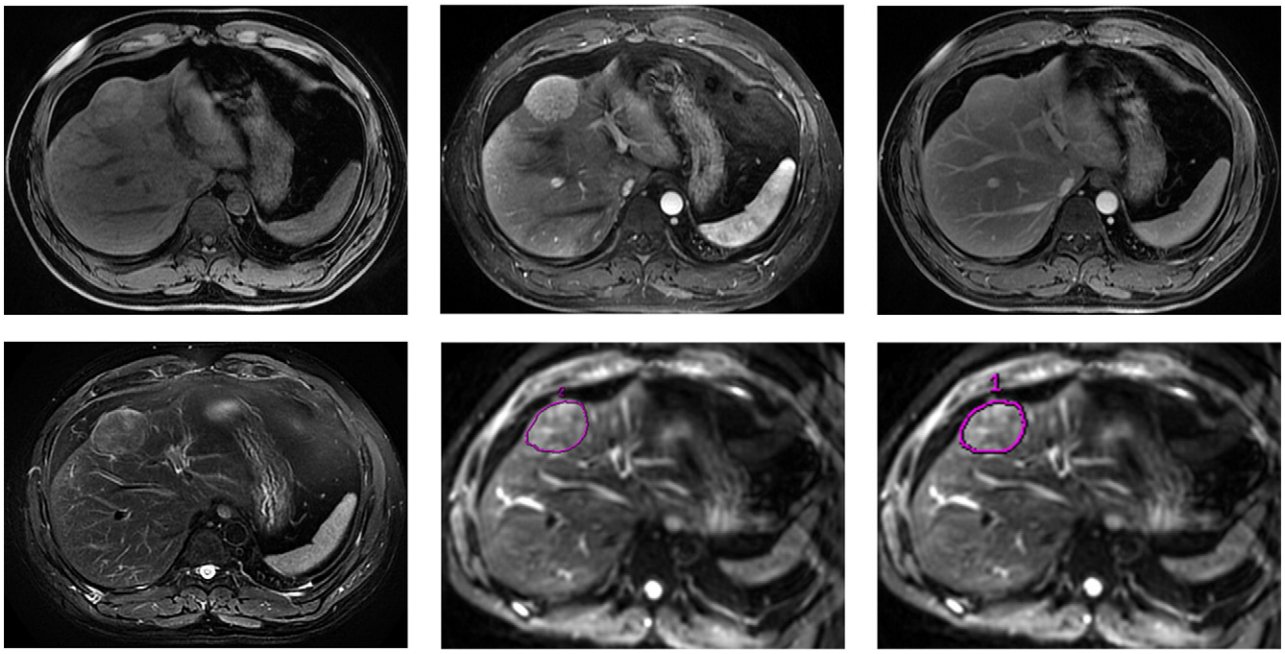

Figure 1. A 33-year-old man with FNH. (A-C) The lesion shows uniform mild hyperintensity on an axial fat-suppressed T1-weighted image in segment IV, homogeneously avid enhancement on the arterial phase, and slow washout on the equilibrium phase, which is a typical imaging manifestation of FNH. (D) Axial fat-suppressed T2-weighted image showing a slightly higher signal intensity. (E) For a homogeneous lesion, a freehand ROI was delineated carefully on the b_0 image to encapsulate the whole lesion as far as possible. (F) After an interval of 1 week, another freehand ROI for retest is delineated to encompass the entire lesion along its border. Both ROIs seem to be identical in appearance. Their coverages are 1587 mm^2 and 1704 mm^2, respectively.

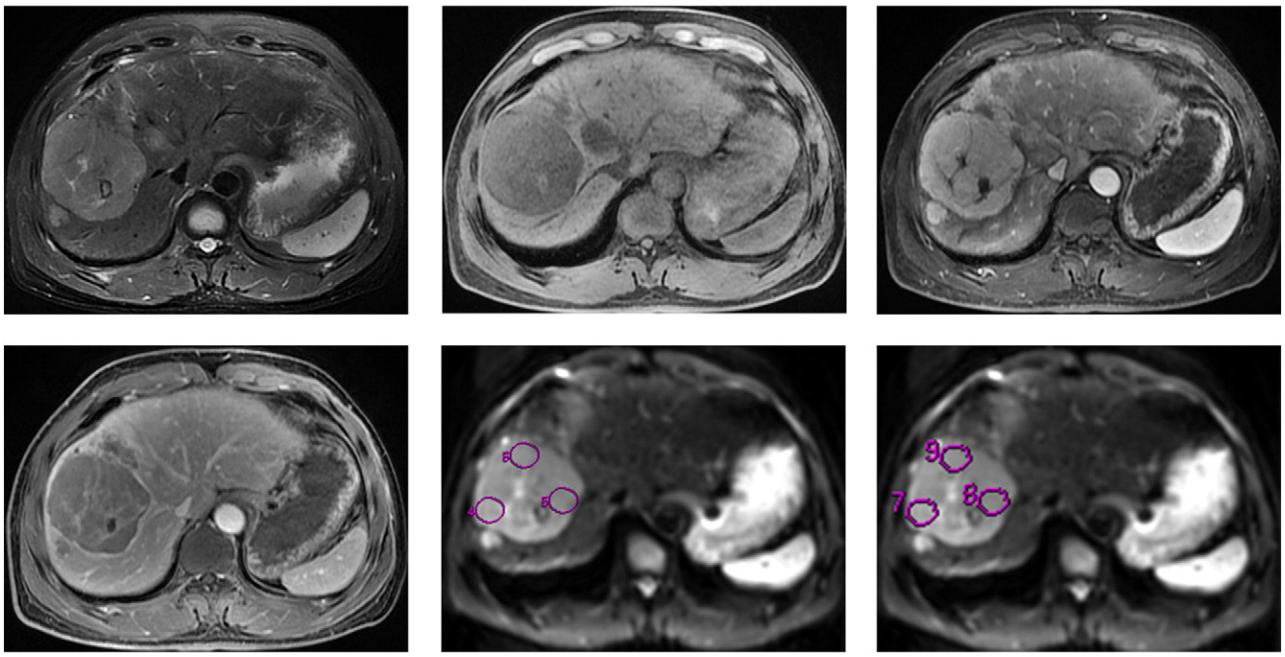

Figure 2. A 52-year-old man with HCC. (A) Axial fat-suppressed T2-weighted image showing a well-demarcated, high–signal intensity lesion in right liver lobe, region of internal lower ring area is present. (B) The lesion shows heterogeneous hypointensity on an axial fat-suppressed T1-weighted image, with region of internal higher signal intensity representing hemorrhage. (C and D) Postcontrast images demonstrate characteristic wash-in and washout on the arterial phase and the equilibrium phase, respectively, which is a typical imaging manifestation of HCC; the central part without enhancement indicates its hemorrhagic nature. (E) For a heterogeneous lesion, three circular ROIs of the same size were set on solid and viable tumor areas on a b_0 image, according to regular MRI sequences; it was meticulous to avoid internal foci of the "hemorrhagic zone". (F) After an interval of 1 week, another three identical ROIs for retest were placed. Both ROIs seem to be identical in appearance, their coverages are almost the same.

where S_0 = signal intensity at b_0 and S_b = signal intensity for a given b value; because D^* was markedly larger than D, D was calculated by the following equation if the b value was greater than 200 s/mm^2, indicating that the perfusion content had almost decayed completely at this setting:

$$S_b/S_0 = \exp.(-bD) \quad (2)$$

D^* and f were acquired using the Levenberg-Marquardt method, which fitted S_b for all b values using Eq. (1) with a fixed D. Subsequently, f and D^* were calculated.

Ultimately, the ADC_{total} was calculated by fitting b_0 and all b values that were great than or equal to 200 s/mm^2 (200, 400, 600, and 800 s/mm^2) to a monoexponential model, and the classic ADC equation was expressed as follows:

$$S_b/S_0 = \exp.(-b\mathrm{ADC}) \quad (3)$$

Statistical Analysis

Unless specified, all data are expressed as means ± standard deviations (SDs).

The uniform sizes of the ROIs were copied for heterogeneous lesions, and freehand ROIs were drawn for homogeneous lesions after 1 week for retest analysis. The locations of the ROIs were kept the same as much as possible to avoid measurement bias.

The nonparametric Mann-Whitney U test was used throughout the study to compare parameters between the malignant and benign groups. Parameters showing statistical significance between the two groups were evaluated by a receiver operating characteristic curve (ROC) to assess diagnostic performance. All analyses were performed using SPSS version 19.0 (Chicago, IL). Results with P value less than .05 were considered statistically significant.

Results

According to the signal intensity obtained from the 11 b values in our study, the relationship between them could be described by a biexponential model in each group.

The results of the IVIM parameters and ADC_{total} between these two groups are depicted in Table 1. ADC_{total}, D, and f were all significantly lower in the malignant group than in the benign group ($P < .05$). The ADC_{total} values were (1.24 ± 0.24) × 10^{-3} mm^2/s and (2.12 ± 0.54) × 10^{-3} mm^2/s in malignant and benign group, respectively. The D values were (0.96 ± 0.19) × 10^{-3} mm^2/s and (1.66 ± 0.35) × 10^{-3} mm^2/s, respectively, and the f values were 19.21% ± 7.38% and 26.55% ± 14.08%, respectively. The D^* values did not show a significant difference between these two types ($P > .05$); the D^* values were (73.28 ± 42.02) × 10^{-3} mm^2/s and (97.89 ± 78.82) × 10^{-3} mm^2/s, respectively (Figures 3 and 4). The comparison between HCC and hemangioma is demonstrated in Table 2 and shows a similar distinction between the malignant and benign groups.

The ROC analysis showed that ADC_{total} and D could be used to distinguish benign from malignant FLLs with an excellent diagnostic ability, whereas f was inferior to ADC_{total} and D (Figure 5). The maximum area under the curve (AUC) value for D was 0.968, followed by ADC_{total} at 0.959 and f at 0.647. When the threshold was set to 1.73 × 10^{-3} mm^2/s and 1.19 × 10^{-3} mm^2/s for ADC_{total} and D, respectively, the highest sensitivity was obtained correspondingly (Table 3).

Table 1. Comparison of IVIM-Derived Parameters and ADC_{total} between Benign and Malignant Group

	Benign	Malignant	*P* Value
ADC_{total} (×10^{-3} mm^2/s)	2.12 ± 0.54	1.24 ± 0.24	.000*
D (×10^{-3} mm^2/s)	1.66 ± 0.35	0.96 ± 0.19	.000*
D^* (×10^{-3} mm^2/s)	97.89 ± 78.82	73.28 ± 42.02	.428
f (%)	26.55 ± 14.08	19.21 ± 7.38	.024*

* Mann-Whitney U test for differences in IVIM parameters and ADC_{total} between benign and malignant group.

Discussion

The results of the present study showed that ADC_{total}, D, and f, especially the former two parameters, are useful to differentiate benign and malignant FLLs. The values for ADC_{total}, D, and f were in line with, or similar to, those reported previously [9,11,12]. We also found that HCC and hemangioma, the most common malignant and benign liver tumors, demonstrated different results that ADC_{total}, D, and f were significantly higher in hemangioma, whereas D^* did not reach statistical significance. Different from the two b values from DWI that ADC is calculated from monoexponential model containing both diffusion and perfusion, and some of the IVIM-related parameters can distinguish these two components using multiple b values by biexponential model [11,13].

Primovist must be injected first for adequate hepatocyte uptake; therefore, some patients were submitted to IVIM acquisition after administration of this contrast agent. Several previous studies observed that the effect of contrast medium on imaging parameters did not have statistical significance and that the image quality was not susceptible to be compromised [14,15]; therefore, our results are credible and are not influenced by the contrast agent.

Malignant FLLs are characterized by a heterogeneous structure; therefore, it is recommended to set several ROIs of the same size in these lesions to avoid necrosis and tortuous vessels [16]. In our study, however, we observed that some of benign lesions did not manifest a homogeneous appearance. This was mainly because of the different pathological changes that could also occur in benign lesions, such as thrombus or phlebolith in hemangioma, cystic change in angioleiomyolipoma, and a central scar in FNH. Thus, the ROI placement for heterogeneous lesions in our study was based on the standard, including setting multiple ROIs to avoid covering nonsolid areas and placing manually uniform ROIs at almost identical locations each time, then calculating their average. Our results demonstrated that the SD of D^* was largest among the parameters, which indicated that D^* was unstable and fluctuating inherently, as was reported by other studies, suggesting that the error in the calculation of D^* is high [17,18] despite maintaining identical ROIs during each operation in the study.

We excluded hepatic cysts during patient selection, although some other studies included them in the benign groups [11–13], and the ADC and D values for benign lesions were significantly larger than those for malignant ones. The reasons that we ruled out hepatic cysts were as follow: First, it is meaningless to make a differentiation between a cyst and noncyst lesion because no contrast enhancement could be observed in a cyst, which is a typical and obvious feature that differs from solid lesions. Moreover, cysts do not actually lack perfusion. Interestingly and peculiarly, they demonstrate "blood circulation" in some cases, despite a lack of enhancement. Yamada et al. were the first to investigate the IVIM on abdominal organs and

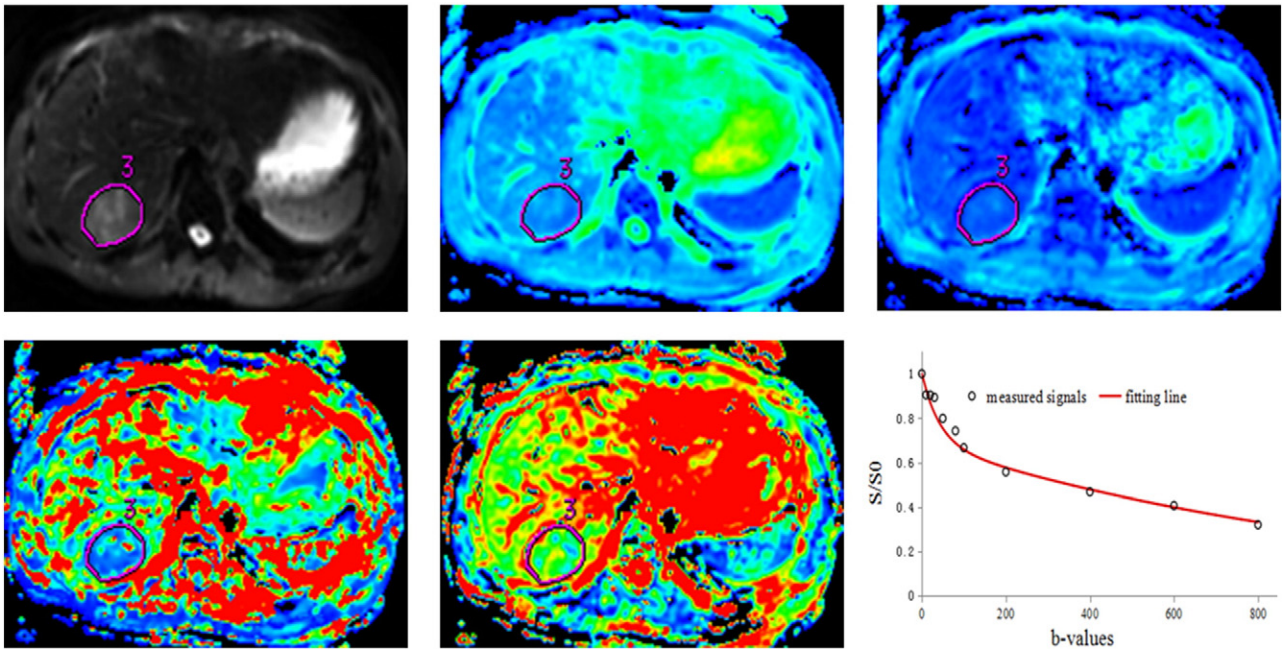

Figure 3. IVIM DW images with 11 *b* values (in the range 0-800 s/mm^2) from a 49-year-old man with HCC. (A) The DW image and a freehand ROI are delineated. Parametric images benefited the presentation of (B) ADC_{total} 1.58 × 10^{-3} mm^2/s, (C) *D* 0.911 × 10^{-3} mm^2/s, (D) D^* 23.6 × 10^{-3} mm^2/s, and (E) *f* 31.3%. (F) Signals decayed biexponentially with the *b* value, as shown by the fitting curve (red line). At low *b* values (<200 s/mm^2), the fitting curve demonstrates a large slope, whereas at large *b* values (>200 s/mm^2), the fitting curve demonstrates a gradually declining curve.

reported that the estimation of perfusion fraction of cysts was 0, meaning that cysts did not have a perfusion component [19]. By contrast, other studies reported that the D^* and *f* of cysts were nonzero [13,20]. It is possible that liver cysts are susceptible to be affected by a flowing-spin effect such that both the liver and the cyst fluctuate because of breath movement. It was likely that, during

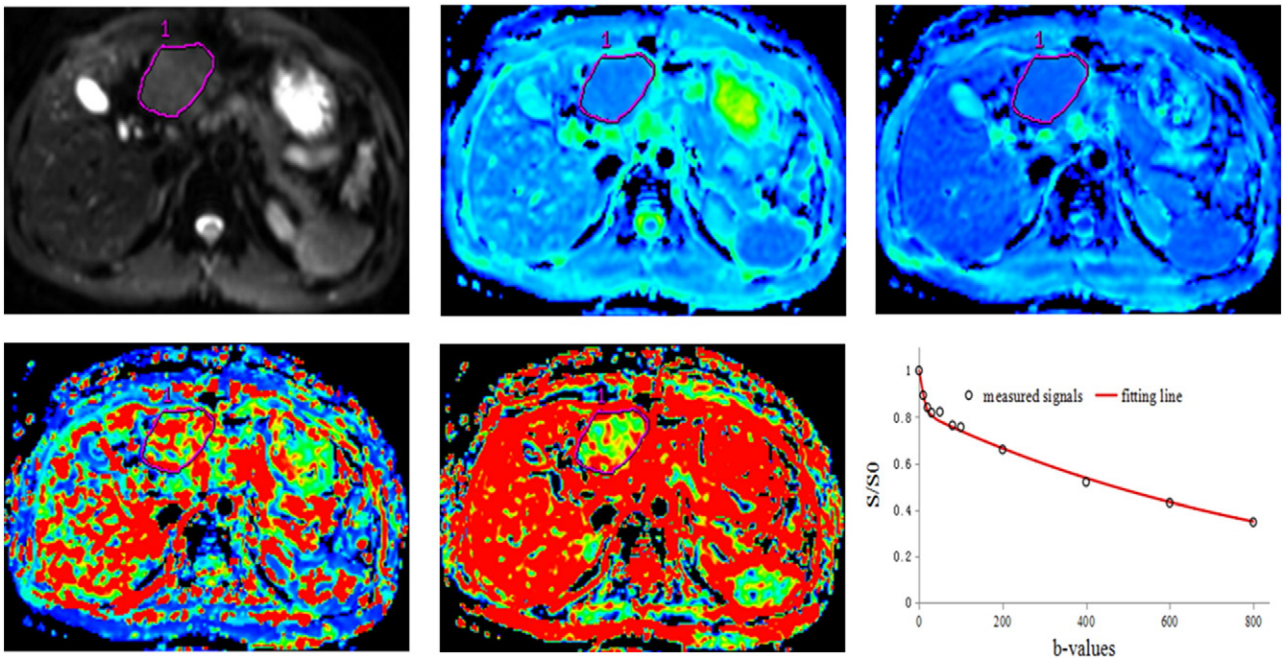

Figure 4. IVIM DW images with 11 *b* values (in the range 0-800 s/mm^2) from a 36-year-old man with FNH. (A) The DW image and a freehand ROI are outlined. Parametric images facilitated the presentation of (B) ADC_{total} 1.45 × 10^{-3} mm^2/s, (C) *D* 1.07 × 10^{-3} mm^2/s, (D) D^* 97.5 × 10^{-3} mm^2/s, and (E) *f* 19.7%. (F) Signals decayed biexponentially with the *b* value, as shown by the fitting curve (red line). At low *b* values (<200 s/mm^2), the fitting curve demonstrates a large slope, whereas at large *b* values (>200 s/mm^2), the fitting curve demonstrates a gradually declining curve.

Table 2. Comparison of IVIM-Derived Parameters and ADC_{total} between Hemangioma and HCC

	Hemangioma	HCC	*P* Value
ADC_{total} ($\times 10^{-3}$ mm^2/s)	2.27 ± 0.51	1.22 ± 0.23	.000*
D ($\times 10^{-3}$ mm^2/s)	1.78 ± 0.32	0.94 ± 0.18	.000*
D^* ($\times 10^{-3}$ mm^2/s)	71.57 ± 53.29	75.49 ± 42.57	.429
f (%)	27.99 ± 16.02	18.78 ± 7.39	.044*

* Mann-Whitney *U* test for differences in IVIM parameters and ADC_{total} between hemangioma and HCC.

scanning, even though the cyst was static and the patient held their breath or breathed regularly, lasting turbulent flow resulting from inertial force might cause a flowing-spin effect. Breath-hold, RT, and free-breathing (FB) might potentially make this effect prominent for their breath capture when generating images. The misregistration resulted from a motion artifact, especially for lesions near the edge of the liver or in the anterior abdominal wall, which could also be attributed to this result even in the absence of perfusion in liver cysts. Thus, these results proved the instability of perfusion parameters from another perspective. Without cyst disturbance, it is more accurate to make a differentiation using solid hepatic tumors.

Different number of *b* values, which varied among studies, could influence the result to some extent. We used 11 *b* values, and 8 to 12 *b* values were used in other studies [10–12]. Larger numbers of small *b* values (<200 s/mm^2) benefit parameter measurement and higher accuracy because if there are too few of them, perfusion parameters could be underestimated [21]. Most studies comprised seven to nine small *b* values [9,13]. Recently, a new concept termed "two key *b* values" has been suggested [22], which indicates that a "low" key *b* value can be identified around 100 to 200 s/mm^2 for IVIM (perfusion) and a "high" one is ≥800 s/mm^2 for non-Gaussian diffusion, contributing to shortening the acquisition time dramatically. Technologically, there are various IVIM image acquisition methods including FB and RT [11,23]. RT is used widely and routinely, producing higher image quality; however, the parametric reproducibility of FB is higher because more excitations can be added and cyclical respiration does not result in additional signal attenuation during scanning. There is still no consensus as to which method is better because many researches have obtained excellent and reasonable results using different methods. Crucially, it should be noted that despite its widespread use and rapid image acquisition, EPI's intrinsic artifacts, such as distortion and ghosting, cannot be eliminated or overlooked completely. With regard to lesion sample size and categories, different studies contained different sample sizes. Our sample was comprised mainly HCC and hemangioma because of their higher morbidity; however, the lesion categories in the study of Doblas et al. were comprised of rare types [9]. The number of HCC and hemangioma cases in our group was lower than that of Yoon et al. [11] and higher than that of Ichikawa et al. [12]. However, unlike the present study, those researches did not make a comparison between them. In addition, we excluded cysts, as discussed above. The number of other FLLs, such as FNH and AML, also varied among reports because of their rarity. Besides, the underlying state of the organ, such as liver fat content, fibrotic tissue fraction, and even fasting or not, could potentially affect these discrepancies [24–26].

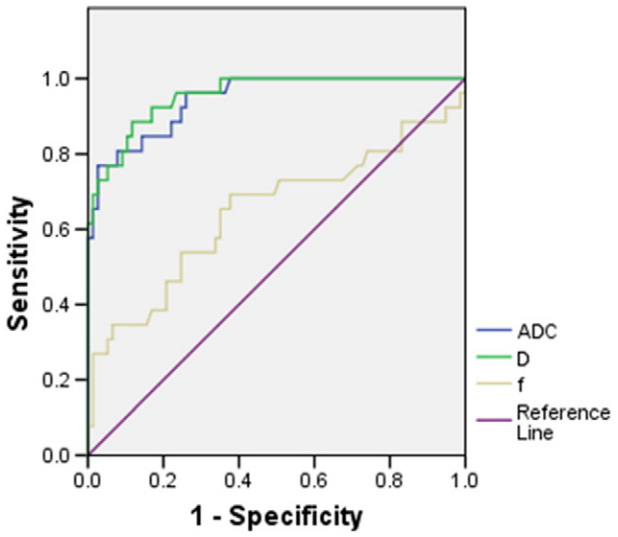

Figure 5. ROC curve generated according to the ADC and *D* values. The cutoff values for ADC and *D* were determined as 1.73 × 10^{-3} mm^2/s and 1.19 × 10^{-3} mm^2/s for hepatic solid benign and malignant tumors, respectively. At an ADC of 1.73 × 10^{-3} mm^2/s, the sensitivity for the prediction was 80.80%. At a *D* value of 1.19 × 10^{-3} mm^2/s, the sensitivity for the prediction was 92.30%. The ROC curves showed that *D* had a slightly higher AUC than ADC.

IVIM could be used as a valuable tool to differentiate between malignant and benign FLLs. Malignant lesions tend to have a more complicated microstructure, including hypercellularity, high nucleus-cytoplasm ratios, and polarity change due to their rapid growth and denser cells, and thus lowered degree or direction of diffusion compared with benign lesions. In addition, swelling in the cell matrix and accumulation of macromolecular substances resulting from high rates of biosynthesis cause architectural changes that could also explain the significantly higher ADC and *D* in benign lesions compared with the malignant ones, which resulted in smaller extracellular spaces and hampered diffusion degree.

Malignant lesions are prone to destroy the parenchyma, invade hepatic vessels, and generate tortuous tumor vessels and immature tissues within these lesions, which have a potential influence on the blood supply to the liver. Although thrombus or cystic change in some of benign lesions leads to a heterogeneous appearance and even arteriovenous shunts or inflammatory congestive reactions are observed, they do not disrupt the surrounding tissue and vasculature; therefore, the remainder of the liver maintains normal structure. The primary pathological change of these lesions is dilated blood sinus in hemangioma [1], disorganized hepatocytes and malformed bile ducts in FNH [27], and variations in the content of fat and thick- or thin-walled vessels mixed together in AML [28]. The different pathological changes and discrepancies in perfusion effects between the two groups could reasonably account for why *f*, the IVIM perfusion parameter, was significantly higher in benign FLLs than in malignant ones.

D^*, another perfusion parameter, was to some extent contradictive to *f*. Both of them provide perfusion information; therefore, they should have a proportional relationship. Nevertheless, they emphasize inconsistent characteristics of perfusion: D^* is correlated with the segment length and velocity of capillary network, whereas *f* measures the fractional blood volume of microcirculation that accounts for all diffusion movement in voxels [29]. Some other studies have observed similar mismatches between D^* and *f* [7,8,30,31]. Importantly, the intrinsic instability of perfusion parameters, particularly D^*, as shown by its high SD, could be attributed to this paradox, especially when

Table 3. ROC Analysis of ADC_{total} and *D* for Prediction and Diagnostic Performance between Benign and Malignant Group

	AUC	Cutoff ($\times 10^{-3}$ mm^2/s)	Sensitivity (%)
ADC_{total}	0.959	1.73	80.80
D	0.968	1.19	92.30

NOTE: Because the AUC value of *f* is significantly smaller than ADC_{total} and *D*, the cutoff and sensitivity of *f* do not calculate.

measured in malignant lesions, which are more heterogeneous. Furthermore, *f* is susceptible to be affected by other bulk flow phenomena, such as glandular secretion, which is difficult to distinguish from perfusion effects, and blood flow pattern, which is not specific to perfusion [21,32]. Vortex and turbulent flow in a hemangioma could influence the penetration and distribution of perfusion. FNH contains bile ducts; therefore, delayed biliary excretion is possible. Additionally, the difference in TE caused by irregular respiration rates or variations in liver sizes for each patient, or accompanying by a peripheral inflammatory reaction that is characterized by vasodilation and increased permeability [33], and a background state of liver cirrhosis could also have delicate influence on parameter measurement [26]. Fortunately, the designed perfusion metric $f \times D^*$ seems to show more stability and better application prospects [34,35], resulting in this metric being recommended by several studies. Further study is warranted to confirm its efficacy.

Our results showed that ADC_{total}, *D*, and *f* remain credible to discriminate between HCC and hemangioma, which contradicts the results of certain other studies [9,10,13]. Scattered thrombi reducing blood filling, and dilated hepatic sinusoid and irregular flowing pattern slowing down the bloodstream could contribute to this discrepancy. Besides, some studies found that perfusion of a liver tumor was related to its location and various blood supply types [10,36]. It should also be noted that both FNH and AML display hypervascularity compared with hypovascular lesions, such as metastatic lesions; there was no apparent perfusion parametric change before and after the elimination of metastasis in the malignant group. Therefore, in some cases, excluding hypervascular lesions could reduce or mask the difference in perfusion parameters between groups.

Some studies stated that the effectiveness of ADC to diagnose and distinguish was limited to some extent because of its nonspecific features, containing both pure diffusion and perfusion [11,35,37]. However, other studies indicated that ADC could be a more useful biomarker than *D* to differentiate disease entities [9,23]. Thus, there is no consensus surrounding these two values. Our results support the view that the discriminatory efficiency of *D* slightly exceeds that of ADC_{total}. The sensitivity of *D* was higher than that of ADC_{total}. *D* is a pure-diffusion parameter that is uniquely sensitive to molecular diffusion; therefore, for the detection of malignant lesions characterized by diffusion restriction, theoretically, *D* is more sensitive than ADC_{total}. Additionally, *D* eliminates the effect of the perfusion component, whereas ADC, as a compound parameter, is more direct for *D* to reflect cell density and the extent of diffusion limitation. Therefore, the AUC of *D* was larger than that of ADC. The SD of *f* was larger than ADC_{total} and *D* despite the significant differences between malignant and benign lesions, suggesting that the practical efficacy of *f* was inferior to ADC_{total} and *D*. However, the potential value of *f* to evaluate and predict tumor response to treatment, such as that shown in hepatic chemotherapy and parotid radiation therapy, has not been eclipsed [38,39].

Our study had several limitations. First, our study may have some selection bias. In contrast to HCC and hemangioma, the sample numbers of FNH and AML in the benign group and metastasis in the malignant group were small because of the low morbidity in the disease spectrum in daily work. Second, the pathology for some patients was not acquired. Nevertheless, the diagnostic criteria for those cases without proven histology were based on their typical imaging features and their relevant laboratory tests. Moreover, it has been noted that different histological grades of HCC could result in different parameters [40]; however, this topic was not pursued because it was beyond the scope of our study. Third, some ROIs were set in the left liver lobe. Lesions located in the left lobe are prone to be influenced by adjacent organs, such as the heart, diaphragm motion, or gastrointestinal peristalsis [41,42]; therefore, it is recommended to select lesions located in the right liver lobe for more stable and accurate estimation [43]. Finally, judging from current IVIM scanning technologies, further studies on the effects of different acquisition methods on IVIM parameters are warranted to form standard guidelines.

Conclusion

Our results show that the ADC_{total} and IVIM diffusion parameter *D*, which provide superior diagnostic performance, could be helpful and reliable to differentiate malignant and benign liver tumors. *D* also shows a higher sensitivity to detect malignant lesions.

Conflict of Interest

All authors declare that there is no conflict of interest.

This research did not receive any specific grant from funding agencies in the public, commercial, or not-for-profit sectors.

References

[1] Cogley JR and Miller FH (2014). MR imaging of benign focal liver lesions. *Radiol Clin N Am* **52**, 657–682.

[2] Bruegel M, Holzapfel K, Gaa J, Woertler K, Waldt S, Kiefer B, Stemmer A, Ganter C, and Rummeny EJ (2008). Characterization of focal liver lesions by ADC measurements using a respiratory triggered diffusion-weighted single-shot echo-planar MR imaging technique. *Eur Radiol* **18**, 477–485.

[3] Koh DM, Scurr E, Collins D, Kanber B, Norman A, Leach MO, and Husband JE (2007). Predicting response of colorectal hepatic metastasis: value of pretreatment apparent diffusion coefficients. *AJR Am J Roentgenol* **188**, 1001–1008.

[4] Le Bihan D, Breton E, Lallemand D, Aubin ML, Vignaud J, and Laval-Jeantet M (1988). Separation of diffusion and perfusion in intravoxel incoherent motion MR imaging. *Radiology* **168**, 497–505.

[5] Marzi S, Forina C, Marucci L, Giovinazzo G, Giordano C, Piludu F, Landoni V, Spriano G, and Vidiri A (2015). Early radiation-induced changes evaluated by intravoxel incoherent motion in the major salivary glands. *J Magn Reson Imaging* **41**, 974–982.

[6] Xiao Y, Pan J, Chen Y, Chen Y, He Z, and Zheng X (2015). Intravoxel incoherent motion-magnetic resonance imaging as an early predictor of treatment response to neoadjuvant chemotherapy in locoregionally advanced nasopharyngeal carcinoma. *Medicine* **94**, e973.

[7] Luciani A, Vignaud A, Cavet M, Nhieu JT, Mallat A, Ruel L, Laurent A, Deux JF, Brugieres P, and Rahmouni A (2008). Liver cirrhosis: intravoxel incoherent motion MR imaging—pilot study. *Radiology* **249**, 891–899.

[8] Klauss M, Mayer P, Maier-Hein K, Laun FB, Mehrabi A, Kauczor HU, and Stieltjes B (2016). IVIM-diffusion-MRI for the differentiation of solid benign and malign hypervascular liver lesions—evaluation with two different MR scanners. *Eur J Radiol* **85**, 1289–1294.

[9] Doblas S, Wagner M, Leitao HS, Daire JL, Sinkus R, Vilgrain V, and Van Beers BE (2013). Determination of malignancy and characterization of hepatic tumor type with diffusion-weighted magnetic resonance imaging: comparison of apparent diffusion coefficient and intravoxel incoherent motion-derived measurements. *Investig Radiol* **48**, 722–728.

[10] Zhu L, Cheng Q, Luo W, Bao L, and Guo G (2015). A comparative study of apparent diffusion coefficient and intravoxel incoherent motion-derived parameters for the characterization of common solid hepatic tumors. *Acta Radiol* **56**, 1411–1418.

[11] Yoon JH, Lee JM, Yu MH, Kiefer B, Han JK, and Choi BI (2014). Evaluation of hepatic focal lesions using diffusion-weighted MR imaging: comparison of apparent diffusion coefficient and intravoxel incoherent motion-derived parameters. *J Magn Reson Imaging* **39**, 276–285.

[12] Ichikawa S, Motosugi U, Ichikawa T, Sano K, Morisaka H, and Araki T (2013). Intravoxel incoherent motion imaging of focal hepatic lesions. *J Magn Reson Imaging* **37**, 1371–1376.

[13] Watanabe H, Kanematsu M, Goshima S, Kajita K, Kawada H, Noda Y, Tatahashi Y, Kawai N, Kondo H, and Moriyama N (2014). Characterizing focal hepatic lesions by free-breathing intravoxel incoherent motion MRI at 3.0 T. *Acta Radiol* **55**, 1166–1173.

[14] Colagrande S, Mazzoni LN, Mazzoni E, and Pradella S (2013). Effects of gadoxetic acid on quantitative diffusion-weighted imaging of the liver. *J Magn Reson Imaging* **38**, 365–370.

[15] Kinner S, Umutlu L, Blex S, Maderwald S, Antoch G, Ertle J, Gerken G, and Lauenstein TC (2012). Diffusion weighted MR imaging in patients with HCC and liver cirrhosis after administration of different gadolinium contrast agents: is it still reliable? *Eur J Radiol* **81**, e625–e628.

[16] Wagner M, Doblas S, Daire JL, Paradis V, Haddad N, Leitão H, Garteiser P, Vilgrain V, Sinkus R, and Van Beers BE (2012). Diffusion-weighted MR imaging for the regional characterization of liver tumors. *Radiology* **264**, 464–472.

[17] Andreou A, Koh DM, Collins DJ, Blackledge M, Wallace T, Leach MO, and Orton MR (2013). Measurement reproducibility of perfusion fraction and pseudodiffusion coefficient derived by intravoxel incoherent motion diffusion-weighted MR imaging in normal liver and metastases. *Eur Radiol* **23**, 428–434.

[18] Patel J, Sigmund EE, Rusinek H, Oei M, Babb JS, and Taouli B (2010). Diagnosis of cirrhosis with intravoxel incoherent motion diffusion MRI and dynamic contrast-enhanced MRI alone and in combination: Preliminary experience. *J Magn Reson Imaging* **31**, 589–600.

[19] Yamada I, Aung W, Himeno Y, Nakagawa T, and Shibuya H (1999). Diffusion coefficients in abdominal organs and hepatic lesions: evaluation with intravoxel incoherent motion echo-planar MR imaging. *Radiology* **210**, 617–623.

[20] Moteki T and Horikoshi H (2006). Evaluation of hepatic lesions and hepatic parenchyma using diffusion-weighted echo-planar MR with three values of gradient b-factor. *J Magn Reson Imaging* **24**, 637–645.

[21] Cohen AD, Schieke MC, Hohenwalter MD, and Schmainda KM (2015). The effect of low b-values on the intravoxel incoherent motion derived pseudodiffusion parameter in liver. *Magn Reson Med* **73**, 306–311.

[22] Iima M and Le Bihan D (2016). Clinical intravoxel incoherent motion and diffusion MR imaging: past, present, and future. *Radiology* **278**, 13–32.

[23] Liu J, Wan Y, Wang Z, Qi Y, Qu P, and Liu Y (2016). Perfusion and diffusion characteristics of endometrial malignancy based on intravoxel incoherent motion MRI at 3.0 T: comparison with normal endometrium. *Acta Radiol* **57**, 1140–1148.

[24] Guiu B, Petit JM, Capitan V, Aho S, Masson D, Lefevre PH, Favelier S, Loffroy R, Vergès B, Hillon P, et al (2012). Intravoxel incoherent motion diffusion-weighted imaging in nonalcoholic fatty liver disease: a 3.0-T MR study. *Radiology* **265**, 96–103.

[25] Hollingsworth KG and Lomas DJ (2006). Influence of perfusion on hepatic MR diffusion measurement. *NMR Biomed* **19**, 231–235.

[26] Parente DB, Paiva FF, Oliveira Neto JA, Machado-Silva L, Figueiredo FA, Lanzoni V, Campos CF, do Brasil PE, Gomes Mde B, Perez Rde M, et al (2015). Intravoxel incoherent motion diffusion weighted MR imaging at 3.0 T: assessment of steatohepatitis and fibrosis compared with liver biopsy in type 2 diabetic patients. *PLoS One* **10**e125653.

[27] Ringe KI, Husarik DB, Sirlin CB, and Merkle EM (2010). Gadoxetate disodium–enhanced MRI of the liver: part 1, protocol optimization and lesion appearance in the noncirrhotic liver. *AJR Am J Roentgenol* **195**, 13–28.

[28] Cohan RH and Ellis JH (2015). Renal masses: imaging evaluation. *Radiol Clin N Am* **53**, 985–1003.

[29] Le Bihan D (2008). Intravoxel incoherent motion perfusion MR imaging: a wake-up call. *Radiology* **249**, 748–752.

[30] Yan C, Xu J, Xiong W, Wei Q, Feng R, Wu Y, Liu Q, Li C, Chan Q, and Xu Y (2017). Use of intravoxel incoherent motion diffusion-weighted MR imaging for assessment of treatment response to invasive fungal infection in the lung. *Eur Radiol* **27**, 212–221.

[31] Hectors SJ, Wagner M, Besa C, Bane O, Dyvorne HA, Fiel MI, Zhu H, Donovan M, and Taouli B (2016). Intravoxel incoherent motion diffusion-weighted imaging of hepatocellular carcinoma: is there a correlation with flow and perfusion metrics obtained with dynamic contrast-enhanced MRI? *J Magn Reson Imaging* **44**, 856–864.

[32] Shinmoto H, Tamura C, Soga S, Shiomi E, Yoshihara N, Kaji T, and Mulkern RV (2012). An intravoxel incoherent motion diffusion-weighted imaging study of prostate cancer. *AJR Am J Roentgenol* **199**, W496–W500.

[33] Deng Y, Li X, Lei Y, Liang C, and Liu Z (2016). Use of diffusion-weighted magnetic resonance imaging to distinguish between lung cancer and focal inflammatory lesions: a comparison of intravoxel incoherent motion derived parameters and apparent diffusion coefficient. *Acta Radiol* **57**, 1310–1317.

[34] Yu XP, Hou J, Li FP, Wang H, Hu PS, Bi F, and Wang W (2016). Intravoxel incoherent motion diffusion weighted magnetic resonance imaging for differentiation between nasopharyngeal carcinoma and lymphoma at the primary site. *J Comput Assist Tomogr* **40**, 413–418.

[35] Shen N, Zhao L, Jiang J, Jiang R, Su C, Zhang S, Tang X, and Zhu W (2016). Intravoxel incoherent motion diffusion-weighted imaging analysis of diffusion and microperfusion in grading gliomas and comparison with arterial spin labeling for evaluation of tumor perfusion. *J Magn Reson Imaging* **44**, 620–632.

[36] Fan ZH, Chen MH, Dai Y, Wang YB, Yan K, Wu W, Yang W, and Yin SS (2006). Evaluation of primary malignancies of the liver using contrast-enhanced sonography: correlation with pathology. *AJR Am J Roentgenol* **186**, 1512–1519.

[37] Kang KM, Lee JM, Yoon JH, Kiefer B, Han JK, and Choi BI (2014). Intravoxel incoherent motion diffusion-weighted MR imaging for characterization of focal pancreatic lesions. *Radiology* **270**, 444–453.

[38] Lewin M, Fartoux L, Vignaud A, Arrivé L, Menu Y, and Rosmorduc O (2011). The diffusion-weighted imaging perfusion fraction *f* is a potential marker of sorafenib treatment in advanced hepatocellular carcinoma: a pilot study. *Eur Radiol* **21**, 281–290.

[39] Zhou N, Chu C, Dou X, Li M, Liu S, Zhu L, Liu B, Guo T, Chen W, He J, et al (2016). Early evaluation of irradiated parotid glands with intravoxel incoherent motion MR imaging: correlation with dynamic contrast-enhanced MR imaging. *BMC Cancer* **16**, 865.

[40] Woo S, Lee JM, Yoon JH, Joo I, Han JK, and Choi BI (2014). Intravoxel incoherent motion diffusion-weighted MR imaging of hepatocellular carcinoma: correlation with enhancement degree and histologic grade. *Radiology* **270**, 758–767.

[41] Schmid-Tannwald C, Jiang Y, Dahi F, Rist C, Sethi I, and Oto A (2013). Diffusion-weighted MR imaging of focal liver lesions in the left and right lobes. *Acad Radiol* **20**, 440–445.

[42] Kwee TC, Takahara T, Niwa T, Ivancevic MK, Herigault G, Van Cauteren M, and Luijten PR (2009). Influence of cardiac motion on diffusion-weighted magnetic resonance imaging of the liver. *MAGMA* **22**, 319–325.

[43] Dijkstra H, Baron P, Kappert P, Oudkerk M, and Sijens PE (2012). Effects of microperfusion in hepatic diffusion weighted imaging. *Eur Radiol* **22**, 891–899.